Single Crystal AlScN-on-Silicon XBAW RF Filter Technology for Wide Bandwidth, High Frequency 5G and WiFi Applications
(Invited)

J.B. Shealy, C. Moe, J. Leathersich, F. Bi, D. Kim, P. Patel, K. Cheema, A. Kochhar, E. Mehdizadeh and M. Winters

Akoustis Technologies, Inc. Huntersville, NC USA, jshealy@akoustis.com

Keywords: AlScN, BAW, Resonators, RF Filters, MOCVD, Si-MEMS

Abstract

This paper demonstrates the first growth and fabrication of wide bandwidth BAW Resonators and RF Filters using single crystal Aluminum Scandium Nitride (AlScN) piezoelectric films grown on 150-mm <111> silicon substrates by MOCVD. Epitaxial $Al_{0.8}Sc_{0.2}N$ films with $Al_{0.2}Ga_{0.8}N$ interlayers with overall thickness of approximately 400 nm were engineered for low stress and high crystalline alignment with 0.38° FWHM measured by XRD. With a unique wafer transfer flow BAW process (XBAW) utilizing the single crystal films, $Al_{0.8}Sc_{0.2}N$ and $Al_{0.75}Sc_{0.25}N$, resonators were fabricated at 4.62 GHz and 7.04 GHz, showcasing FoM of 140 and 124, respectively. These new single crystal resonators were used to demonstrate PCM RF filters using a ladder configuration of four series and three shunt resonators. Finally, RF power measurements indicated a consistent 2-dB improvement in power handling over filters constructed using physical vapor deposited (PVD) material in the same XBAW process.

INTRODUCTION

Next generation of wireless standards, such as 5G and WiFi 6E, are expected to enhance device performance and enable new applications while drastically increasing number of bands and the bandwidth of wireless communication systems. These are enabled by high-performance acoustic Micro-Electro-Mechanical (MEMS) filters [1-3]. To achieve optimal acoustic filter performance within newly allocated frequency spectrum, trade-offs between power, frequency and bandwidth of RF resonators must be engineered. One such engineering "knob" is the starting piezoelectric layer which has historically been constructed using PVD-based, polycrystalline films. For wideband applications, scandium-doped aluminum nitride has commercially covered the much-needed bandwidth requirement both at mid and high frequency spectrum. From a volume manufacturing aspect, the major drawbacks are the PVD target material's fixed concentration requirement and costs, as Sc content increases. Additionally, fixed concentrations provide discrete values of k_{eff}^2, impacting filter design approach. From an application aspect, the power requirement has always been demanding for access points, small cell, and infrastructure deployments.
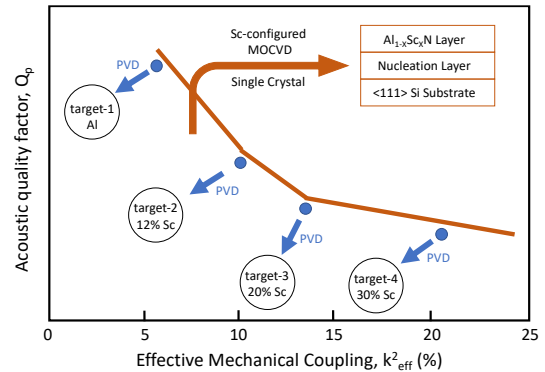

Fig 1. Motivation of MOCVD (single crystal PZ) growth compared to PVD (poly crystal PZ) growth to achieve wide range of resonator coupling.

The key metric for it is the power handling capability of BAW resonators, which is dependent on the crystal quality of the piezoelectric material and its effect on thermal conductivity. Higher Sc concentrations tend to show lower thermal conductivities [4]. However, due to microstructural material differences between single crystal and polycrystalline films, the thermal conductivity for bulk quality single crystal material has been shown to outperform polycrystalline sputtered piezoelectric films [5-7]. Our prior work demonstrated at 3.6 GHz exhibited 2.6 dB power improvement for single crystal AlN piezoelectric films compared to polycrystalline AlN [8]. As the MOCVD deposition technique can achieve continuous and optimal coupling values by adjusting Sc-gas flow in the growth reactor (Fig. 1) to control the Sc content while producing material with lower defect density, the above key aspects get addressed.

In this work, we explore Sc-alloy AlN (AlScN) piezoelectric (PZ) layers manufactured using MOCVD to achieve wide bandwidth, high frequency BAW RF filters and showcase the key performance of XBAW products.

MOCVD GROWTH OF SINGLE CRYSTAL ALSCN FILMS

Highly Sc-doped AlScN film structures were grown in a multi-wafer, 150-mm configured MOCVD system onto Si <111> substrates. First, a nucleation layer was first deposited to ensure a wurtzite crystal structure, with AlGaN layers with

increasing Ga concentrations then grown to produce a compressive film stress during growth. AlScN was then deposited using TMAl, NH$_3$ and a proprietary, commercially available metal-organic Sc source.
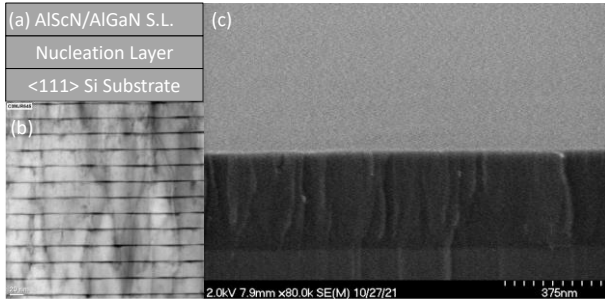

Fig 2. (a) Piezoelectric material stack grown for this study, (b) TEM cross-section of single crystal Al$_{0.8}$Sc$_{0.2}$N superlattice and (c) SEM of Al$_{0.8}$Sc$_{0.2}$N surface.
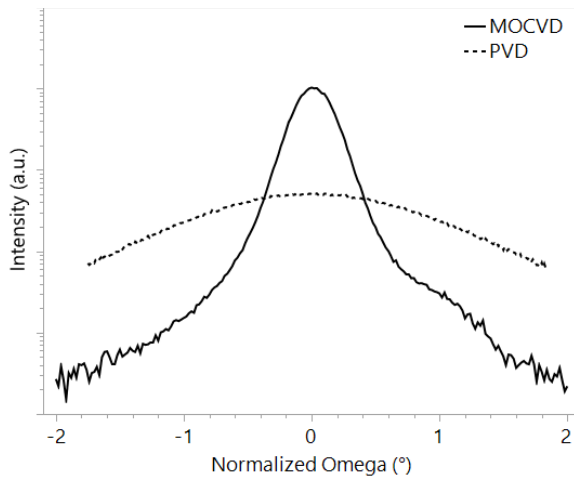

Fig 3. 0002 ω-scan of single crystalline MOCVD-grown (solid line) and polycrystalline PVD-grown (dotted line) Al$_{0.8}$Sc$_{0.2}$N films.
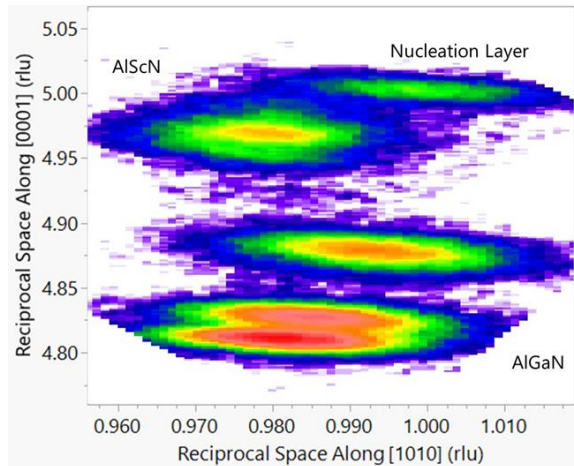

Fig 4. Reciprocal space map in the 10-15 direction of the as-grown AlScN structure, showing the nucleation layer, AlGaN stress-mitigating layers, and the Al$_{0.8}$Sc$_{0.2}$N resonator layer.

During MOCVD growth of the AlScN layer, it was observed that a combination of the film stress during growth and the low defect density of the films causes an accumulation of Sc atoms on the growth surface in a mechanism similar to that observed in InGaN growth by MOCVD [9]. This accumulated Sc roughens the surface and results in a three-dimensional film morphology unsuitable for further processing. To prevent this, 2 nm-thick Al$_{0.2}$Ga$_{0.8}$N interlayers were deposited in 20 nm intervals to maintain a smooth growth surface (Fig 2). The resulting Al$_{0.8}$Sc$_{0.2}$N superlattice was 370 nm in total thickness and had no abnormally oriented grains as is typically observed with PVD films. The full-width half-maximum (FWHM) of the (002) AlScN peak as measured by x-ray diffraction (XRD) was 0.38°, indicating highly ordered, single crystal PZ material. For comparison, typical PVD films of the same thickness have FWHM values of 1.8 to 1.9° as shown in Fig 3. 2θ-ω scans performed by XRD also showed no extraneous diffraction peaks as has been observed in other thick AlScN growth by MOCVD [10], and a reciprocal space map shown in Fig. 4 of the AlGaN/AlScN structure shows the AlScN peak partially strained to the underlying AlGaN layers, but with a c/a ratio smaller than AlN. The epitaxial superlattice structures reported contained either Al$_{0.8}$Sc$_{0.2}$N or Al$_{0.75}$Sc$_{0.25}$N layers, with no difference in XRD FWHM observed between the different alloy compositions. Sc content was verified by SIMS analysis.

DEVICE FABRICATION WITH ALSCN FILM

Wide bandwidth resonators and filters were manufactured combining the single-crystal Al$_{0.8}$Sc$_{0.2}$N and Al$_{0.75}$Sc$_{0.25}$N piezoelectric films with a novel MEMS-based BAW process [11] to achieve the final device structure shown in Fig 5. This unique process allows utilizing an epitaxially grown thin film on a flat seed substrate in a manner that is not possible with conventional BAW resonator manufacturing procedures and includes removing the underlying AlGaN and nucleation layers prior to electrode metallization. The process is versatile such that high performance resonators can be produced from a wide variety of piezoelectric films extending from sputtered polycrystalline AlN to AlScN films with greater 30% Sc content [12][13]. The resonators were tested using on-wafer, 1-port configuration with air coplanar ground-signal probe.
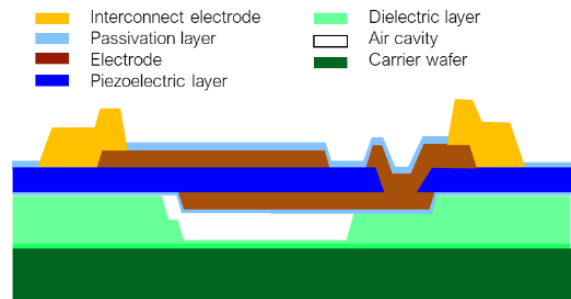

Fig 5. Schematic cross-section of finished XBAW resonator used to fabricate RF filter. The piezoelectric layer consists of MOCVD grown, single crystal AlScN superlattice.
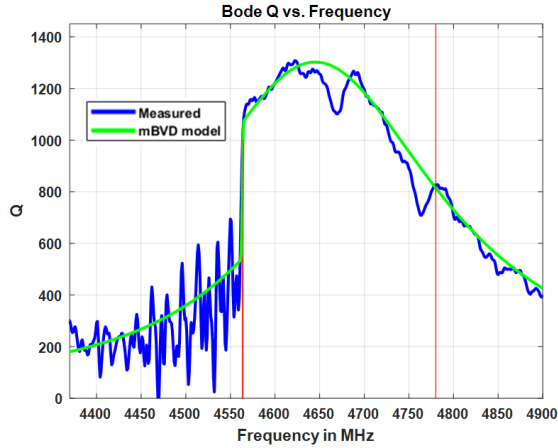
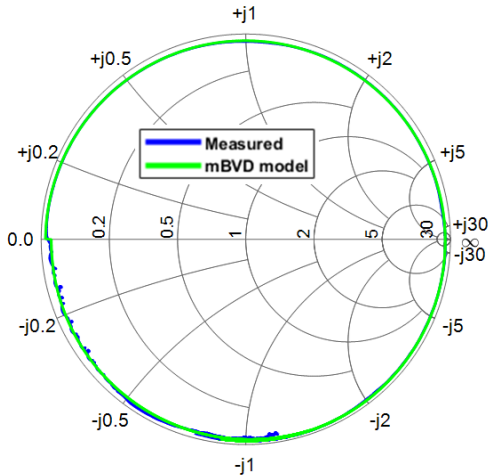Fig 6. Measured Bode plot of Q-curve vs. frequency of single crystal $Al_{0.8}Sc_{0.2}N$ resonator.

Fig 7. Q-circle or S11 plot on a Smith Chart from measured data of single crystal $Al_{0.8}Sc_{0.2}N$ resonator.

The XBAW device using the $Al_{0.8}Sc_{0.2}N$ superlattice was designed for 4.63 GHz and exhibited k_{eff}^2 of 10.7%. The Q Bode of the measured resonator and its mBVD model is evaluated using the method described in [14]. As seen in Fig 6, the Bode plot shows Q_s, Q_p, and Q_{max} of 1150, 820, and 1310, respectively. This translates to a figure of merit (FoM), product of Q_{max} and k_{eff}^2, of 140. Smith chart of the de-embedded measured device overlaying the mBVD fitted electrical network is shown in Fig 7. The XBAW device using the $Al_{0.75}Sc_{0.25}N$ superlattice was designed for 7.04 GHz and exhibited k_{eff}^2 of 11.45%. As seen in Fig 8, the Bode plot shows Q_s, Q_p, and Q_{max} of 600, 831, and 1087, respectively. This translates to FoM of 124. Smith chart of the de-embedded measured device overlaying the mBVD fitted electrical network is shown in Fig 9.

MEASURED FILTER RESULT

The process control monitor (PCM) XBAW RF filter designs were evaluated. The BAW die features a ladder type filter topology of four identical series and three identical shunt resonators (4s3p).
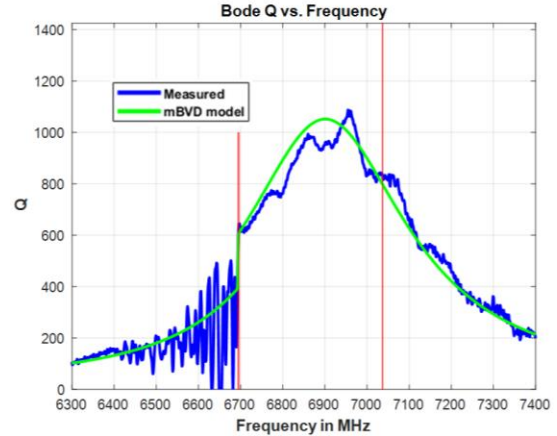

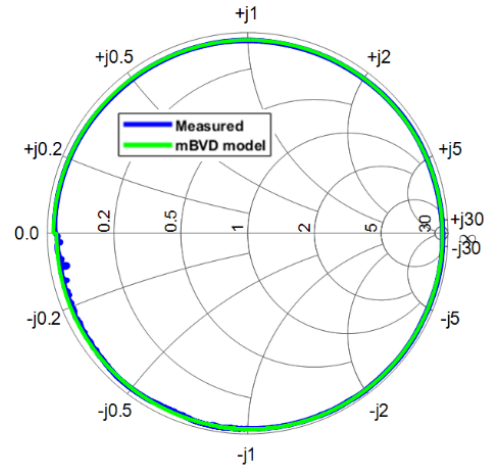Fig 8. Measured Bode plot of Q-curve vs. frequency of single crystal $Al_{0.75}Sc_{0.25}N$ resonator.

Fig 9. Q-circle or S11 plot on a Smith Chart from measured data of single crystal $Al_{0.75}Sc_{0.25}N$ resonator.

The die size is 600 x 350 um^2 and is matched to 50 Ohms using external reactive elements. Fig. 10 shows the measured S21, S11, and S22 response of 4.8 GHz PCM filter using $Al_{0.8}Sc_{0.2}N$ superlattice over the frequency of interest, respectively with insertion loss of 0.78 dB and 3 dB bandwidth of 390 MHz. Fig. 11 shows the S21 response of 7.2 GHz PCM filter using $Al_{0.75}Sc_{0.25}N$ superlattice over the frequency of interest with insertion loss of ~2.2 dB and a -3dB bandwidth of 914 MHz. The centre of passband has higher insertion loss because wide bandwidth was purposely targeted. No spurious modes are observed in both passband and stopband.

Figure 12 depicts the performance of each material in terms of power handling capability, namely, (Pin vs. Pout). A separate PCM 1 stage RF filter, comprising of one series and one shunt resonator (1s1p) was evaluated. For reference, a PVD sputtered $Al_{0.8}Sc_{0.2}N$ (polycrystalline) material was included in the experiment. To maintain consistency in the measurement, frequencies were swept only in 30% of mid-band. The input power is swept from 0 dBm until the failure

of devices through passband collapse were detected. As shown in Fig. 12, mean failures were observed for PVD 20% Sc polycrystalline at 31 dBm, while the MOCVD-grown epitaxial (EPI) material at both Sc compositions at 33 dBm.
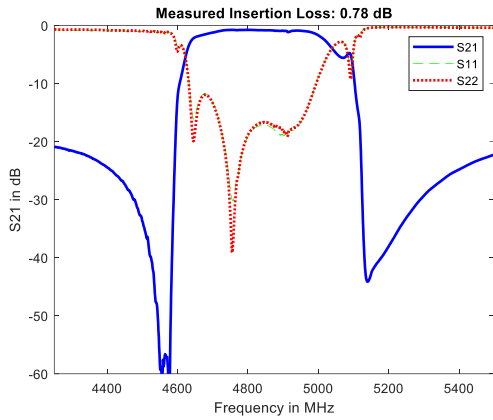

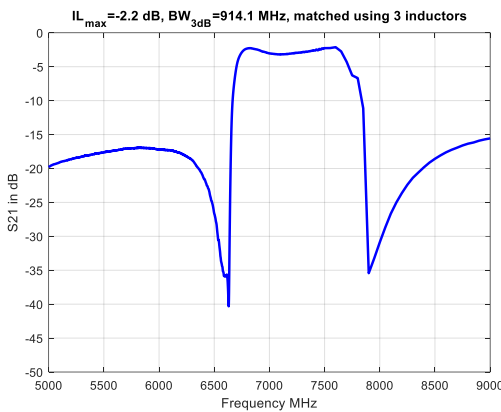Fig 10. Measured S21, S11, S22 response for 4s3p ladder 4.8 GHz PCM RF filter using single crystal $Al_{0.8}Sc_{0.2}N$ piezoelectric film.

Fig 11. Measured S21, S11, S22 response for 4s3p ladder 7.2 GHz PCM RF filter using single crystal $Al_{0.75}Sc_{0.25}N$ piezoelectric film.
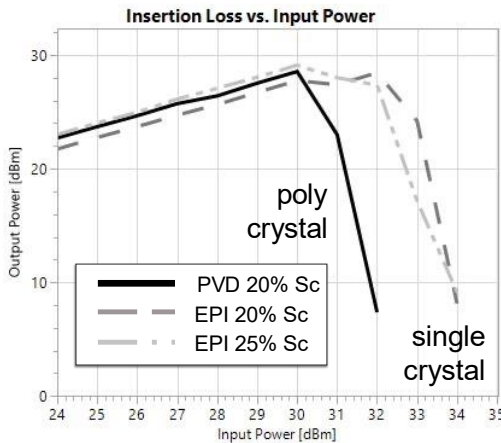

Fig 12. Power measurement using 1s1p PCM RF filter for PVD (polycrystalline) 20% Sc, EPI 20% Sc, and EPI 25% Sc.

CONCLUSION

With a novel wafer transfer BAW (XBAW) process, we report first demonstrations of MOCVD-based $Al_{0.8}Sc_{0.2}N$ and $Al_{0.75}Sc_{0.25}N$ superlattice films. The resulting superlattice films had no abnormally oriented grains as is typically observed with PVD films and are highly ordered with FWHM of 0.38°. The BAW resonators with $Al_{0.8}Sc_{0.2}N$ at 4.63 GHz exhibits FoM of 140 and with $Al_{0.75}Sc_{0.25}N$ at 7.04 GHz, exhibits FoM of 126. No spurious modes are observed in both passband and stopband of the measured filter response. Further, first demonstrators of 4.8 GHz and 7.2 GHz RF filters exhibit impressive low insertion loss and wide bandwidth. Additionally, the power measurements for these films at ~7 GHz demonstrate 2 dB improvement in MOCVD films compared to polycrystalline PVD. In addition to the expected better thermal conductivity in epitaxial films, the superlattice structure and inter-layers utilized to make high crystalline piezoelectric film has contributed to improving the power handling. Finally, these results demonstrate the promise of producing continuous and optimal values of mechanical coupling in AlScN films using Sc-configured MOCVD.

REFERENCES

[1] R. Ruby, *IEEE Microwave Magazine*, vol. 16, no. 7, pp. 46-59, Aug. 2015.
[2] R. Aigner et al, *IEEE IEDM*, pp. 332-335, December 2018.
[3] D. Kim et al., *IEEE MTT-S IMS*, pp. 207-209, 2021.
[4] Yiwen Song et al., *ACS Applied Materials & Interfaces*, 13 (16), 19031-19041, 2021.
[5] B. E. Belkerk et al., Appl. Phys. Lett. 105, 221905 (2014).
[6] Zhe Cheng et al., Phys. Rev. Materials 4, 044602, 2020.
[7] Gustavo Alvarez-Escalante et al., APL Materials 10, 011115 (2022)
[8] Y. Shen etal., *2020 IEEE IUS*, Las Vegas, NV, USA, 2020, pp. 1-3.
[9] K. Pantzas et al, *phys. stat. sol. (a)*, 209, pp. 25-28.
[10] J. Ligl et al, *J. Appl. Phys.* 127, pp. 195704.
[11] R. Vetury et al, *2018 IEEE Int. Ultrason. Symp.*, Oct 2018.
[12] Y. Shen et al, *2019 IEEE Int. Electron Devices Meeting*, San Francisco, CA, USA, 2019, pp. 17.6.1-17.6.4.
[13] M.D. Hodge et al, *IEEE IEDM*, pp625-628, December 2017.
[14] R. Ruby et al, *Proc. of IEEE Ultrason. Symp.*, pp1815-1818, 2008.